Full-zone analysis of relativistic spin splitting at band anticrossings: The case of zinc-blende semiconductors

Athanasios N. Chantis,[1] Niels E. Christensen,[2] Axel Svane,[2] and Manuel Cardona[3]
[1]*Theoretical Division, Los Alamos National Laboratory, Los Alamos, New Mexico 87545, USA*
[2]*Department of Physics and Astronomy, University of Aarhus, DK-8000 Aarhus C, Denmark*
[3]*Max Planck Institut für Festkörperforschung, Heisenbergstrasse 1, D-70569 Stuttgart, Germany*
(Received 22 February 2010; revised manuscript received 13 April 2010; published 12 May 2010)

We show that the band spin splitting caused by spin-orbit interaction in crystal structures with no inversion symmetry is strongly influenced by band anticrossing. The splitting is always enhanced for one of the anticrossing bands and suppressed for the other. There are two limiting cases. In the first, the spin splitting is completely suppressed for one of the bands and doubled for the other. In the second, the absolute value of the splitting is markedly enhanced for both bands approaching the magnitude of the hybridization gap. We demonstrate these effects in zinc-blende semiconductors with the help of first-principles GW calculations.

DOI: 10.1103/PhysRevB.81.205205 PACS number(s): 71.70.Ej, 71.15.Qe

I. INTRODUCTION

In nonmagnetic crystal structures with a center of inversion (e.g., silicon) all electronic band states with a given **k** vector are at least doubly degenerate. In the absence of inversion symmetry (e.g., for GaAs and other zinc-blende structure materials) this degeneracy is lifted by spin-orbit interaction over most of the Brillouin zone (BZ). This splitting was first discussed in 1955 by Dresselhaus[1] for the case of semiconductors with zinc-blende structure, later the discussion was extended to semiconductors with wurtzite crystal structure[2,3] and two-dimensional (2D) semiconductor structures with structural inversion asymmetry.[4,5] It was also early realized, both experimentally[6–8] and theoretically,[9–11] that further lowering of the crystal symmetry by applied uniaxial stress could transform the magnitude and form of the splitting. In a more general picture, the band splitting in all these cases can be viewed as a spin splitting caused by the action of an effective magnetic field that is created by the relativistic coupling of the quasiparticle momentum to the surrounding environment (crystal or structure potential) under certain conditions of low symmetry. From this point of view, the aforementioned band splittings in semiconductors are only one demonstration of a more general relativistic phenomenon. For example, the action of the effective magnetic field in magnetic metallic surfaces is to shift the spin-split bands in opposite directions of the BZ.[12]

This relatively small relativistic effect has attracted much attention since the 1980s, when several experimental determinations of the spin splitting in the vicinity of the zone center of semiconductors were performed.[6,13–18] The effect was also measured in quantum well structures[19–22] and metal surfaces.[12,23,24] The interest in this effect is growing because it is associated with a large number of single-particle and many-body phenomena that occur in semiconductors and metals. We mention here the spin relaxation in doped semiconductors[25] and semiconductor nanostrucutres,[26] tunneling anisotropic magnetoresistance in ferromagnet/semiconductor junctions,[27,28] weak antilocalization in semiconductor 2D structures,[29] quantum spin hall effect,[30] spontaneous polarization of photoelectrons in semiconductors,[13] and unconventional superconducting pairing in the newly discovered class of noncentrosymmetric heavy fermionic superconductors[31] (see also Ref. 32 and references therein).

Theoretically, it is well understood that the effective magnetic field depends on the magnitude and orientation of the quasiparticle momentum and the symmetry of the band state.[22] It is customary to analyze the effect within the framework of the Dresselhaus[1] and Bychkov-Rashba[4] approaches. These involve expansion of the band energies to terms of third order in the components of k in the vicinity of band extrema where the band states usually have well-defined symmetry. However, little is known to this date about the properties of the relativistic spin splittings far from these high-symmetry points. The properties of a quasiparticle in an arbitrary band energy state located at a general point in the BZ can be strongly influenced by interband coupling and therefore only multiband calculations with a realistic crystal potential provide an accurate result in the full BZ. Full zone calculations were presented in Refs. 11, 33, and 34 and most recently in Ref. 35. These calculations showed that the magnitude of spin splitting changes wildly throughout the BZ. A specific region in the vicinity of the [210] direction with maximum spin splitting of the lowest conduction band was identified in Ref. 35. The existence of such a region was generally attributed to interband coupling.[34,35]

In this work we analyze the spin splitting at band anticrossings for an arbitrary point in the BZ. We show that around k points where bands anticross regions of the BZ appear where the spin splitting of the anticrossed bands is largely enhanced or suppressed by spin-mixing band hybridization. The extent of these regions and the effects of enhancement or suppression are discussed in detail within a two-band model Hamiltonian and the first-principles quasiparticle self-consistent GW (QSGW) calculations of the energy bands of GaAs, AlAs, InSb, and CdTe. These calculations confirm that the maximum splitting of the lowest conduction band takes place along the [110] directions *provided one stays within the range of validity of the* k^3 approximation. However, with increasing k the maximum splits into two when one approaches the regions of anticrossing be-

tween the first and second conduction bands. The shape of regions of enhanced spin splitting and the magnitude of enhancement differs from material to material. The observed differences are fully explained with the two-band model Hamiltonian. The results of this analysis apply to the general case of relativistic splitting at band anticrossings, whether this occurs in semiconductors or metals, in three- or two-dimensional geometry, and are not limited to a specific form of the effective magnetic field (be it Dresselhaus, Rashba or strain).

II. COMPUTATIONAL METHOD

The spin-orbit splitting under consideration strongly depends on band parameters such as the energy gap between the first and second conduction bands and the gap between the top valence band and the lowest conduction band.[11,34] In the local-density approximation (LDA) these gaps are in large disagreement with experiment. It was shown in Ref. 34 that the strong underestimation of the fundamental gap in GaAs by LDA leads to a spin splitting parameter that is 14 times bigger than the value predicted from a band structure that has the correct gap. Therefore, in this work we use the recently developed QSGW approximation[36,37] implemented in the full potential linear muffin-tin orbital (LMTO) method.[38,39] The method and the results for a variety of materials are described in great detail in Refs. 34, 36, 37, and 40–43. In the Appendix we describe how this method is applied here and provide detailed comparison of the calculated quasiparticle energies with experiment and with accurate empirical methods (EMs) (see Fig. 1 and Table I in the Appendix). The good agreement of calculated band energies with experimental values at all points of high symmetry in the BZ indicates that the entire calculated band structure (ground and excited states) is very close to that of the real materials throughout the entire BZ. This gives us enough confidence to calculate the spin-orbit splittings of valence and conduction bands throughout the entire BZ.

III. RESULTS

We would like first to give a very brief summary of most important first-principles results relevant to this discussion. In Figs. 2 and 3 we present the full zone spin splitting for the first (CB1) and second conduction band (CB2) for four different semiconductors. It is seen that in all cases the spin splitting of CB1 is maximized in a "banana-shaped" region close to the [210] direction (InSb shows an additional maximum at the W point of the BZ). These regions are in one-to-one correspondence with the regions in the BZ where CB1 and CB2 anticross (see Fig. 11 in the Appendix). The exact shape and extent of these regions varies from material to material, CdTe having the widest banana-shaped region and InSb the thinest. In the same regions the splitting of CB2 does not always experience a maximum. In some cases it is even suppressed. A similar behavior of the spin splitting at band anticrossings was also found for the hole bands.

To understand the large enhancement of the spin splitting for CB1 and CB2 at the points of anticrossing we construct

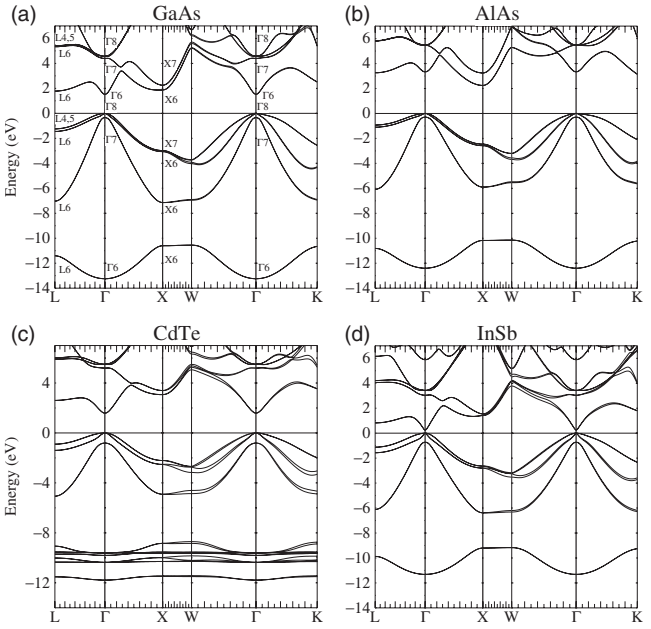

FIG. 1. The calculated band structure of GaAs, AlAs, InSb, and CdTe. For comparison with experimental data at high-symmetry points in the BZ see Table I in the Appendix. The good agreement of calculated band energies with experimental values at all points of high symmetry in the BZ indicates that the entire calculated band structure (ground and excited states) is very close to that of the real materials throughout the entire BZ..

the following two-band noninteracting Hamiltonian:

$$H = H_0 + H_{SO} + H_\Delta, \tag{1}$$

where H_0 is the spin-diagonal part,

$$H_0 = \sum_{\mathbf{k}} \epsilon_1(\mathbf{k}) c_{\mathbf{k}}^+ c_{\mathbf{k}} + \sum_{\mathbf{k}} \epsilon_2(\mathbf{k}) d_{\mathbf{k}}^+ d_{\mathbf{k}}, \tag{2}$$

H_{SO} is the intraband relativistic effective-field part

$$H_{SO} = \sum_{\mathbf{k}} c_{\mathbf{k}}^+ [\mathbf{A_1}(\mathbf{k}) \cdot \boldsymbol{\sigma}] c_{\mathbf{k}} + \sum_{\mathbf{k}} d_{\mathbf{k}}^+ [\mathbf{A_2}(\mathbf{k}) \cdot \boldsymbol{\sigma}] d_{\mathbf{k}} \tag{3}$$

and H_Δ is the hybridization of the two bands, which in the most general case includes a spin-mixing hybridization (similar to an interband H_{SO} term)

$$H_\Delta = \sum_{\mathbf{k}} \Delta(\mathbf{k}) c_{\mathbf{k}}^+ d_{\mathbf{k}} + \sum_{\mathbf{k}} c_{\mathbf{k}}^+ [\boldsymbol{\Delta}'(\mathbf{k}) \cdot \boldsymbol{\sigma}] d_{\mathbf{k}} + \text{H.c.}, \tag{4}$$

where $c_{\mathbf{k}}^+ = (c_{\mathbf{k}\uparrow}^+, c_{\mathbf{k}\downarrow}^+)$ and $d_{\mathbf{k}}^+ = (d_{\mathbf{k}\uparrow}^+, d_{\mathbf{k}\downarrow}^+)$ are the two-component spinor fields for the first and the second band, respectively. $\epsilon_{1,2}(\mathbf{k})$ are the band energies for the first and the second bands, $\boldsymbol{\sigma} = (\sigma_x, \sigma_y, \sigma_z)$ are the components of the Pauli matrix, vectors $\mathbf{A_1}$ and $\mathbf{A_2}$ are the relativistic effective fields for the first and the second bands, respectively (for example, $\mathbf{A} \propto [k_x(k_y^2 - k_z^2), k_y(k_z^2 - k_x^2), k_z(k_x^2 - k_y^2)]$ for the case of the Γ_6 representation in zinc-blende semiconductors), $\Delta(\mathbf{k})$ is the magnitude of the spin-diagonal band hybridization and $\boldsymbol{\Delta}'(\mathbf{k})$ is the effective vector field responsible for the spin-mixing band hybridization. In the following we assume that all spin-mixing vector fields are collinear.

TABLE I. Important band energies for AlAs, GaAs, InSb, and CdTe. Experimental data and EM results are taken from Ref. 47. All energies are given in electron volt. The top of the valence band is set to 0. The experimental and EM data include effects of electron-phonon interaction, absent in our calculations (see Table III of Ref. 48). In our calculations we have not included local $p_{1/2}$ orbitals; as it was shown in Ref. 49, this can result in a small underestimation of spin-orbit splitting $E(\Gamma_{8v})-E(\Gamma_{7v})$ in the heavier compounds.

		AlAs	GaAs	InSb	CdTe
Γ_{6v}	QSGW	−12.40	−13.240	−11.32	−9.81
	Expt.		−13.1	−11.7	
	EM	−12.00	−13.10	−11.70	−11.07
Γ_{7v}	QSGW	−0.29	−0.34	−0.8	−0.81
	Expt.	−0.3	−0.341	−0.85	−0.89 at 293 K
	EM	−0.30	−0.341	−0.85	−0.89
Γ_{8v}	QSGW	0	0	0	0
	Expt.				
	EM	0	0	0	0
Γ_{6c}	QSGW	3.33	1.52	0.23	1.58
	Expt.	3.13	1.52	0.235	1.61 at 2 K
	EM	2.95	1.52	0.237	1.60
Γ_{7c}	QSGW	5.45	4.40	3.04	5.19
	Expt.		4.72	3.141	
	EM	4.60	4.72	3.14	5.36
Γ_{8c}	QSGW	5.48	4.58	3.42	5.5
	Expt.			3.533	
	EM	4.67	4.89	3.42	5.59
X_{6v}	QSGW	−10.18	−10.60	−9.2	−8.84
	Expt.		−10.75	−9.5	-8.8 ± 0.3
	EM	−9.56	−10.58	−9.66	−9.11
X_{6v}	QSGW	−5.9	−7.14	−6.39	−4.91
	Expt.		−6.70	−6.4	-4.7 ± 0.2
	EM	−5.63	−6.66	−6.33	−5.05
X_{6v}	QSGW	−2.58	−3.06	−2.80	−2.52
	Expt.			−2.4	
	EM	−2.68	−3.04	−2.64	−2.05
X_{7v}	QSGW	−2.46	−2.98	−2.64	−2.21
	Expt.		−2.80		-1.8 ± 0.2
	EM	−2.50	−2.89	−2.24	−1.60
X_{6c}	QSGW	2.25	1.88	1.41	3.07
	Expt.	2.23	2.18	1.79	
	EM	2.23	2.03	1.71	3.48
X_{7c}	QSGW	3.24	2.26	1.54	3.39
	Expt.		2.54		
	EM	3.84	2.60	1.95	3.94
L_{6v}	QSGW	−10.81	−11.40	−9.87	−9.07
	Expt.		−11.24	−10.5	
	EM	−10.16	−11.16	−10.24	−9.41
L_{6v}	QSGW	−6.07	−7.02	−6.11	−5.06
	Expt.		−6.70		
	EM	−5.35	−6.65	−6.22	−4.86
L_{6v}	QSGW	−1.10	−1.45	−1.57	−1.39
	Expt.			−1.4	
	EM	−1.49	−1.51	−1.49	−1.18
$L_{4,5v}$	QSGW	−0.93	−1.24	−1.12	−0.90
	Expt.		−1.30	−0.9	-0.9 ± 0.3
	EM	−1.30	−1.30	−0.96	−0.65
L_{6c}	QSGW	3.26	1.79	0.82	2.61
	Expt.		1.85		
	EM	2.59	1.82	1.03	2.82

TABLE I. (*Continued.*)

		AlAs	GaAs	InSb	CdTe
L_{6c}	QSGW	5.81	5.34	4.06	5.9
	Expt.			4.32	
	EM	5.68	5.40	3.60	6.18
$L_{4,5c}$	QSGW	5.83	5.41	4.22	6.01
	Expt.			4.47	
	EM	5.74	5.53	3.80	6.37

For an arbitrary point $\mathbf{k}_0$ in the BZ, where we assume there is an avoided crossing of the two bands, the model Hamiltonian can be written as

$$H(k') = \begin{pmatrix} \epsilon_1(k') & -i\alpha_1 & \Delta & -i\delta' \\ i\alpha_1 & \epsilon_1(k') & i\delta' & \Delta \\ \Delta & -i\delta' & \epsilon_2(k') & -i\alpha_2 \\ i\delta' & \Delta & i\alpha_2 & \epsilon_2(k') \end{pmatrix}, \quad (5)$$

where, $\epsilon_{1,2}(k')$ are the band energies for the first and the second bands if there is no band hybridization ($\Delta=\delta'=0$) and relativistic spin splittings ($\alpha_1=\alpha_2=0$). We have introduced $k'=|\mathbf{k}-\mathbf{k}_0|$ and have assumed that in the vicinity of $\mathbf{k}_0$ $\mathbf{A}_{1,2}$, Δ and $\mathbf{\Delta}'$ are independent of k. For simplicity we chose the vectors $\mathbf{A}_{1,2}$ and $\mathbf{\Delta}$ to have the simple form $(0,y,0)$. We have assumed linear isotropic dispersion for the unhybridized bands by setting $\epsilon_1(k')=ak'$ and $\epsilon_2(k')=-bk'$. Note that the symbol a represents the lattice parameter whenever it appears with $(2\pi/a)$ or $(a/2\pi)$. Then for $\Delta=\delta'=\alpha_1=\alpha_2=0$ the Hamiltonian describes the crossing bands in Fig. 4(a) [where we take $a=b=1$ eV $(a/2\pi)$]. For a finite value of the hybridization parameter Δ, the Hamiltonian describes the anticrossing bands in Fig. 4(a) that are split at $k'=0$ by the hybridization gap of $2\Delta=0.5$ eV.

If we turn on the relativistic splittings (for simplicity we consider $\alpha_1=\alpha_2$) we see in Figs. 4(b)–4(d) that in both cases of no hybridization [Fig. 4(b)] and spin-diagonal hybridization [Fig. 4(c)] the bands split by an equal amount due to relativistic terms. The spin splitting is independent of k and Δ. Diagonalization of Hamiltonian (2), at $k'=0$, with $\Delta\neq 0$, $\alpha_1\neq\alpha_2$, and $\delta'=0$, shows that both bands split by an equal amount of $\alpha_1+\alpha_2$. In the unhybridized case ($\Delta=0$), the first band splits by $2\alpha_1$ and the second by $2\alpha_2$. When we choose $\alpha_1=\alpha_2$, it appears as if the spin-diagonal hybridization has no effect on the spin splitting of the bands. In real materials it is not unlikely for the two bands to have comparable relativistic terms. More important, independent of the α_1/α_2 ratio, both bands split by an equal amount which is independent of k. Therefore, the spin-diagonal hybridization does not result in any new interesting behavior of the spin splitting and certainly does not describe the behavior for the realistic bands seen in Figs. 2 and 3.

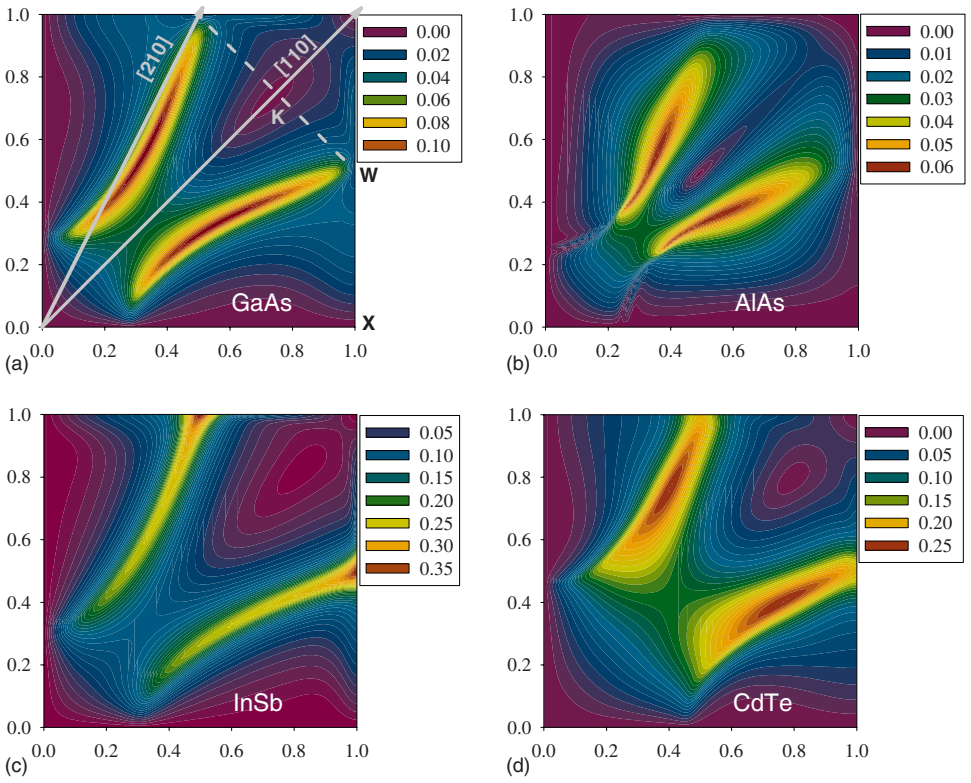

FIG. 2. (Color online) Contour plot of the calculated relativistic splitting of CB1 in one quarter of the [100]-[010] plane in the BZ (the splitting in the other three quarters looks exactly like the one shown above, as expected from the T_d symmetry of the zinc-blende crystal structure). The axes are in units of $(2\pi/a)$. The splitting is given in electron volt.

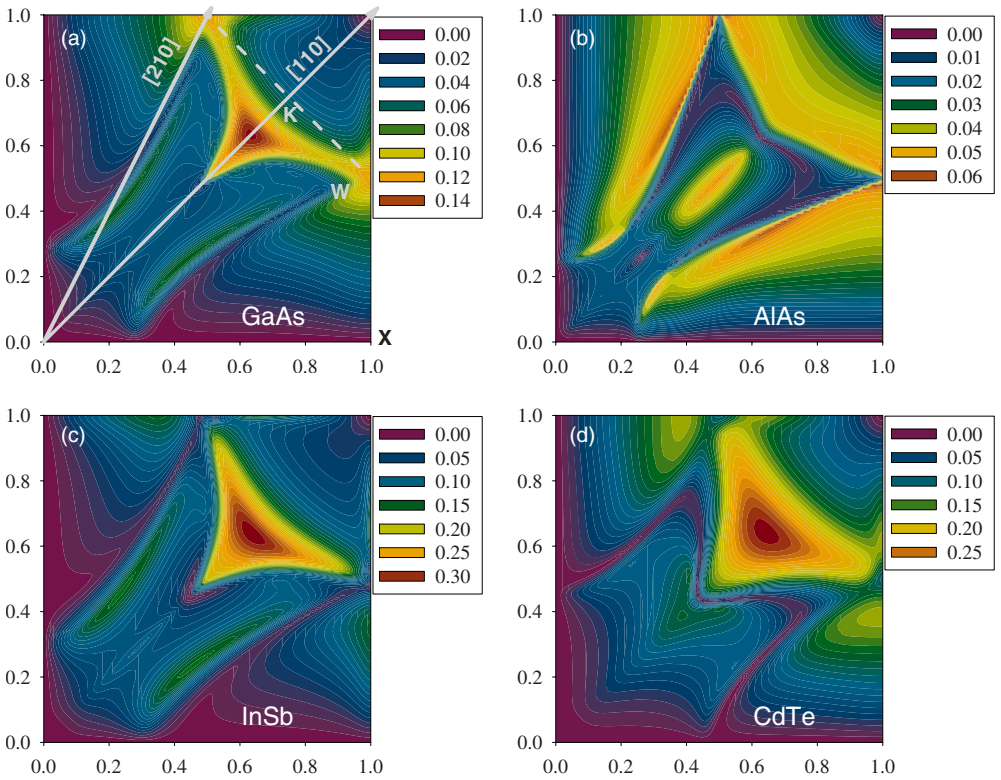

FIG. 3. (Color online) Same as Fig. 1 but for CB2.

We examine now the case of a finite spin-mixing hybridization δ'. The eigenvalues of such a Hamiltonian for $k'=0$ and the case when $\alpha_1=\alpha_2$ are

$$E_{1\pm} = \Delta \pm (\delta' + \alpha_1),$$

$$E_{2\pm} = -\Delta \pm (\delta' - \alpha_1). \tag{6}$$

We have two bands separated by the hybridization gap of 2Δ. The first band is spin split by $(\delta'+\alpha_1)$ and the second by $(\delta'-\alpha_1)$. If δ' is much bigger than α_1 then, the spin splitting of both bands is approximately equal to $2\delta'$. However, as our following comparison of the model with the *ab initio* results will demonstrate, in real materials the spin-mixing hybridization can be comparable to the intraband relativistic terms. In this case, the spin splitting of one band is enhanced and that of the other is suppressed by the hybridization. In the special case of $\delta'=\alpha_1$, the spin splitting of one of the bands is completely suppressed. In the following we examine the eigenvalues of the model Hamiltonian (5) for different values of the model parameters and then compare the calculations with the ab initio results of Figs. 2 and 3.

In Fig. 5 we present the model bands and their spin splitting for $\alpha_1=\alpha_2=-0.01$ eV, $\Delta=0.25$ eV, and $\delta'=0.04\Delta=\alpha_1$. In this special case when the spin-mixing hybridization is equal to the intraband relativistic terms, we see that the spin splitting of one of the bands is completely suppressed at $k=0$ while the spin splitting of the other band is doubled. Here, the suppression occurs for the lower band because we have chosen α_1 and α_2 to be negative (in the opposite case, the suppression occurs for the upper band). Away from $k'=0$ the spin splitting for the lower band is increased with k while that of the upper band is decreased.

In Fig. 6, we show the spin splitting of the lower and upper band for various strengths of spin-mixing hybridization δ'. It is seen that when δ' is significantly larger than the intraband relativistic terms, both bands experience enhancement of spin splitting at the anticrossing point. The enhancement is proportional to the strength of spin-mixing hybridization δ'. *The enhanced splitting can be an order of magnitude bigger than that caused by intraband relativistic*

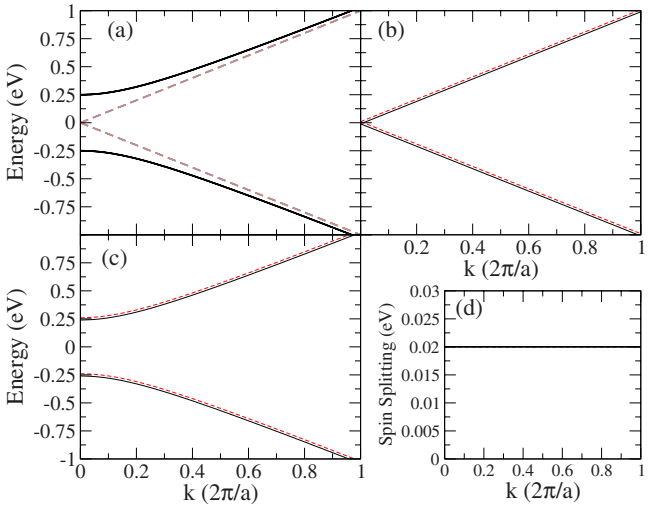

FIG. 4. (Color online) (a) The crossing bands of the model Hamiltonian without [brown (gray) dashed line] and with (black solid line) spin-diagonal hybridization ($\Delta=0.25$ eV), in the case of no relativistic spin splitting. (b) The unhybridized bands with relativistic intraband terms $\alpha_1=\alpha_2=0.01$ eV. (c) The bands with spin-diagonal hybridization ($\Delta=0.25$ eV) and relativistic intraband terms $\alpha_1=\alpha_2=0.01$ eV; (d) the spin splitting for (b) and (c).

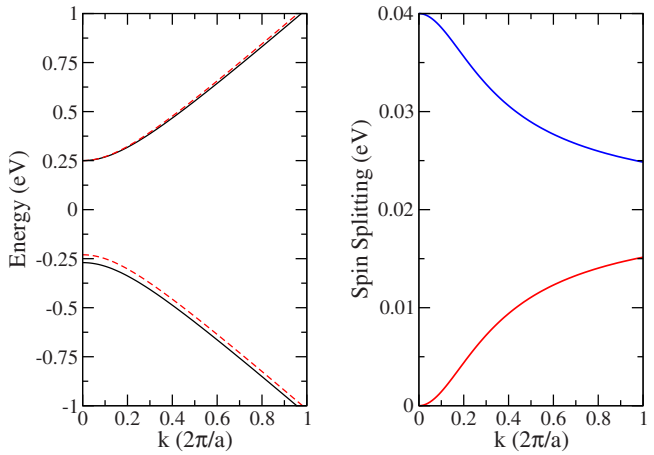

FIG. 5. (Color online) Left panel: the anticrossing bands with relativistic intraband terms and spin-mixing interband hybridization. Right panel: the spin splitting for the lower blue (light gray) line and upper red (dark gray) line bands. The parameters are $a=b=1$ eV$(a/2\pi)$, $\alpha_1=\alpha_2=0.01$ eV, $\Delta=0.25$ eV, and $\delta'=0.04\Delta=\alpha_1=0.01$ eV.

terms. When the spin-mixing hybridization is equal to the spin-conserving hybridization ($\delta'=\Delta$), the spin splitting for both bands is approximately equal to the magnitude of the hybridization gap.

In Fig. 7, we show the dependence of the enhancement on the Bloch velocity $\hbar^{-1}(dE/dk)_{k_0}$ of electrons in the crossing bands. It emerges that the larger the velocity the smaller the extension of the effect in k space. As shown in this figure, by keeping the velocity of one of the bands constant while increasing the velocity of the other, we can achieve a significant change in the width of the peak. For $a=10$ eV$(a/2\pi)$ and $b=1$ eV$(a/2\pi)$ the peak is very narrow. Then, a tenfold increase in the velocity of the second band ($b=10$ eV$(a/2\pi)$) has a significant but much smaller effect. We conclude that *the band with the largest velocity determines the sharpness of the peak in the dependence of the spin splitting on k*.

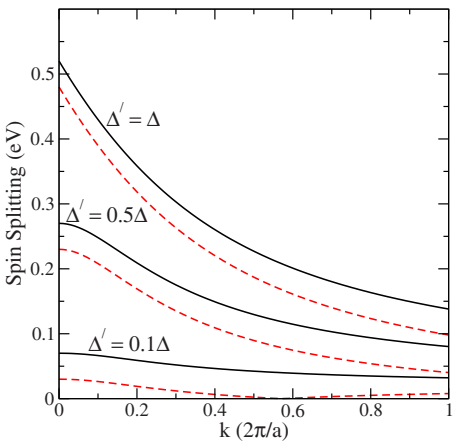

FIG. 6. (Color online) The absolute value of the spin splitting of the lower (red (gray) dashed line) and upper (solid blue (black) line) bands for various strengths of spin-mixing interband hybridization. Here we have chosen $a=b=1$ eV$a/(2\pi)$, $\alpha_1=\alpha_2=0.01$ eV, and $\Delta=0.25$ eV.

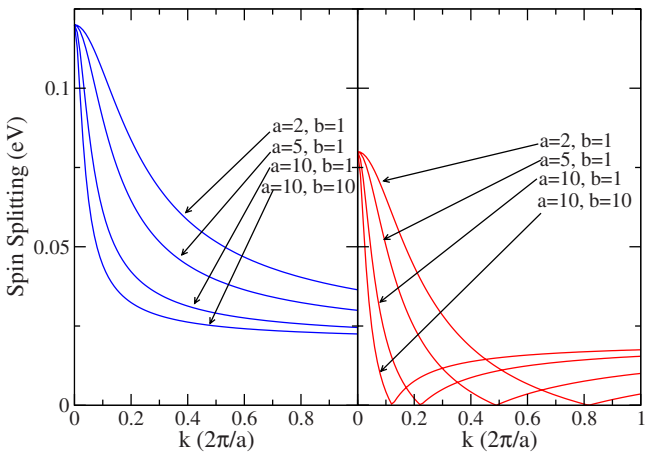

FIG. 7. (Color online) Left panel: the absolute value of the spin splitting of the upper band for different values of coefficients a and b [given here in units of eV$(a/2\pi)$]. Right panel: same as left panel but for the lower band.

It is now interesting to examine the relevance of this model to the realistic bands that we obtained from our first-principles calculations. In Fig. 8, we show a cross section of the two lowest conduction bands and their splitting for GaAs. This cross section is along the line $(k_x,0.5,0)(2\pi/a)$ and we show only a small interval of about $\pm 0.1(2\pi/a)$ around the point of anticrossing of the CB1 and CB2 bands. We urge the reader to identify this interval in the corresponding region in the two-dimensional plots of Figs. 2 and 3. The

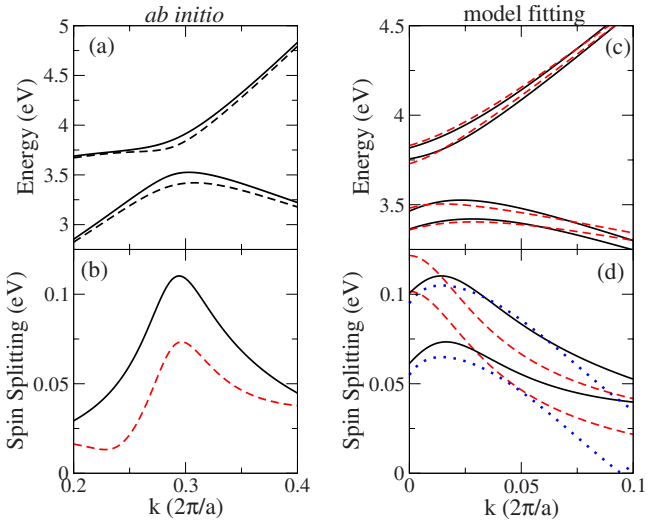

FIG. 8. (Color online) Left panel: cross section of the (a) two lowest conduction bands and (b) their spin splitting for GaAs calculated from first principles. Here $k_y=0.5(2\pi/a)$. Right panel: (c) the model with parameters (independent of k) $\alpha_1=\alpha_2=0.007$ eV, $\Delta=0.18$ eV, $\delta'=0.3\Delta$, $a=9.6$ eV$(2\pi/a)$, and $b=2.5$ eV$(2\pi/a)$ (dashed red(gray) lines) reproduces the main features of the bands calculated from first principles (solid black lines). (d) The model spin splitting (absolute value) with hybridizations Δ and δ' (independent of k) (red(gray) dashed lines), and k-dependent hybridization $\Delta=0.18+ck-c'k^2$ (blue(light gray) dots) are compared to the spin splitting of CB1 and CB2 of first-principles calculations (solid black lines).

spin splitting of both bands is seen to be enhanced at the anticrossing point at around $0.3(2\pi/a)$. On the right panel of Fig. 8 we show the results of fitting the model to the *ab initio* bands. It is evident that the simple model reproduces the main features of the spin-split bands. However, as seen in Fig. 8(d) we find that the model Hamiltonian with k-independent hybridization cannot reproduce the peak of spin splitting, which for the realistic bands is observed at a finite k point away from the anticrossing. We find that this is reproduced by choosing a k-dependent hybridization with the simple form $\Delta=0.18+ck-c'k^2$.

Finally, an interesting question is whether in real materials the spin-mixing hybridization can be as big as the spin-conserving one. For this, in Fig. 9 we present the lowest conduction bands and their spin splitting for CdTe along the same $(k_x,0.5,0)(2\pi/a)$ line in the BZ that we presented results for GaAs above. We see that at $k=0.15(2\pi/a)$, there is a hybridization gap. The spin splitting of both bands is enhanced at this point. *The magnitude of the spin splitting is almost equal to that of the hybridization gap*, as is evidenced by the fact that the spin splitting *nearly closes the gap*. In addition, it is seen that the enhancement is maintained for a large k interval due to the small velocity of the crossing bands, in full accordance with the predictions of our simple model. It is interesting that for very narrow bands such accidental anticrossings will influence the relativistic splitting in very large regions of the BZ. This may be the case for noncentrosymmetric heavy fermionic superconductors, such as $CePt_3Si$, where the entire Fermi-surface (consisting mainly of narrow $4f$ bands) experiences a significant relativistic splitting.[44]

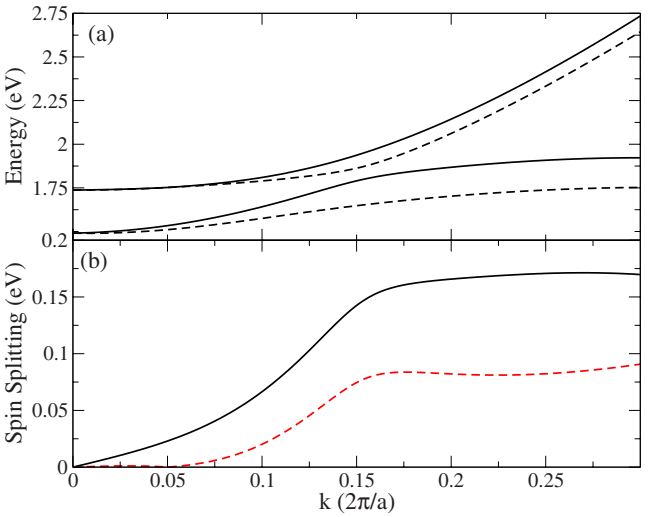

FIG. 9. (Color online) Cross section of the (a) two lowest conduction bands and (b) their spin splitting for CdTe calculated from first principles. Here $k_y=0.5(2\pi/a)$. The spin splitting is approximately equal to the hybridization gap (the gap is almost closed by the spin splitting). The very low velocity of the crossing bands results in a large k interval with enhanced spin splitting.

IV. CONCLUSIONS

We have presented a model of relativistic spin splitting at band anticrossings. We found that the spin splitting of one of the bands is enhanced and that of the other suppressed by the presence of a spin-mixing band hybridization component δ'. The amount of enhancement/suppression is determined by the magnitude of δ'. When $\delta'\approx\alpha_{1,2}$ the splitting for one of the bands can be completely suppressed. When $\delta'\approx\Delta$ the absolute value of the spin splitting is greatly enhanced for both bands and becomes similar in magnitude similar to that of the hybridization gap. *This last case is actually realized in CdTe*. The extent of enhancement/suppression in the BZ is determined by the velocities of the crossing (unhybridized) bands. The smaller the velocity the wider the extent of the

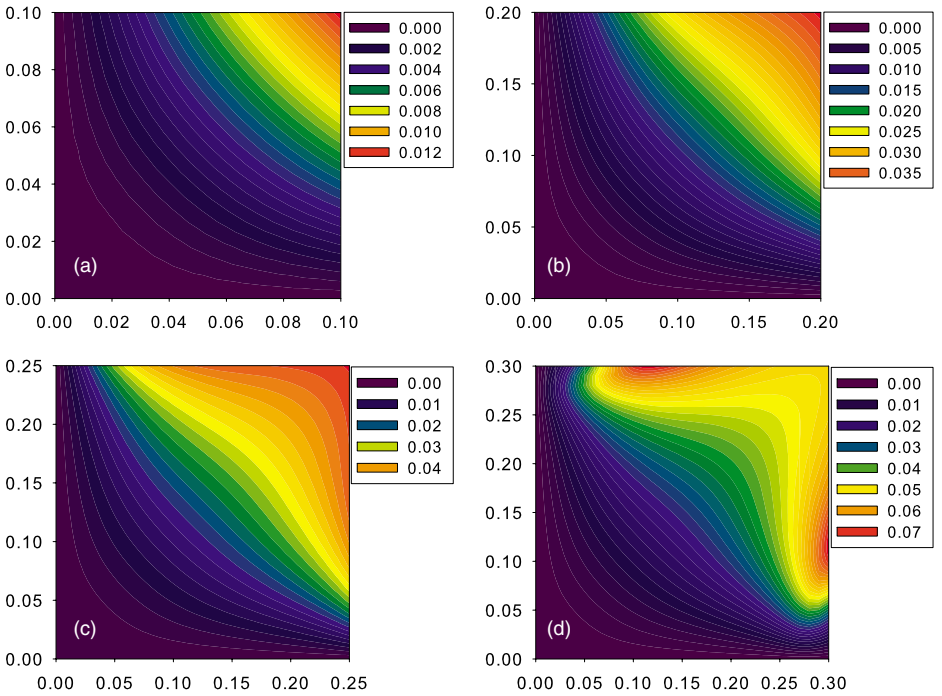

FIG. 10. (Color online) The calculated relativistic splitting of CB1 of GaAs. Notice the different upper limits for k_x and k_y [given in units of $(2\pi/a)$] in the different plots. For small k the maximum is along [110], as k increases the maximum shifts toward the points of CB1 and CB2 anticrossing.

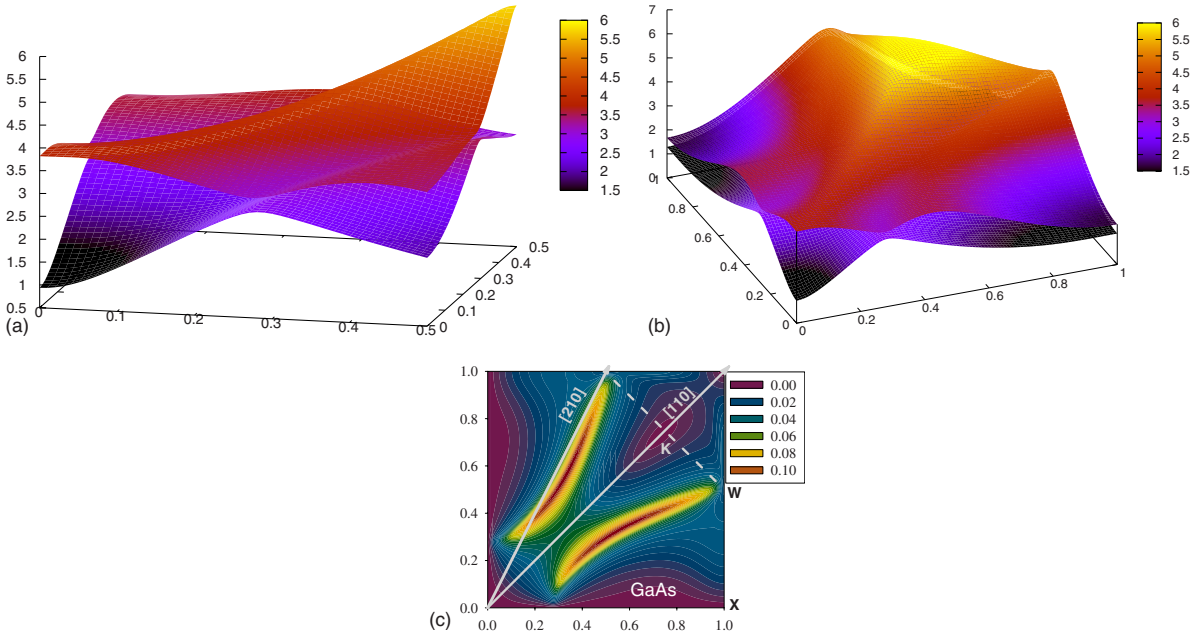

FIG. 11. (Color online) The upper two panels show three-dimensional plots of the CB1 and CB2 dispersion in one quarter of the [100]-[010] plane from two different viewing angles. The plot on the left side is in the range between 0.0 and $0.5(2\pi/a)$ for both k_x and k_y. The plot on the right is for the entire first quarter of the [100]-[010] plane. The lower panel shows the relativistic splitting of CB1 in the same BZ region. It is seen that the relativistic splitting is greatly enhanced at a banana-shaped line where CB1 and CB2 anticross. One of the lines starts approximately at (0.3,0.1,0) and ends at a point nearby (1.0,0.5,0) (W point) (the other line is a mirror reflection of this line). In total there are four such pairs in the entire [100]-[010] plane, consistent with the T_d point group of the zinc-blende structure. The enhancement of spin splitting at k points of band anticrossing is also illustrated in the two-dimenstional plots of Figs. 8 and 9.

effect in the BZ. These findings are supported by the results of first-principles multiband calculations for four different semiconductors. We would like to emphasize that in the model we did not specify the type of spin-orbit splitting or orbital character of the band, therefore we expect that the effects described here occur whenever a band anticrossing takes place under the influence of all types of relativistic effective fields and can be observed for both electrons and holes in semiconductors and metals.

ACKNOWLEDGMENT

The work at Los Alamos National Laboratory was supported by DOE Office of Basic Energy Sciences Work Proposal No. 08SCPE973.

APPENDIX

1. Method: Numerical details and comparison of calculated quasiparticle energies with experiment

For the semiconductors presented in this paper, the smoothed LMTO basis includes orbitals with $l \leq l_{\max}=5$. Two channels of d character were used in the calculations, where the semicore states ($3d$ for Ga and As, $4d$ for Cd, In, Sb, and Te) are added in the form of local orbitals[45]—an orbital strictly confined to the augmentation sphere, which has no envelope function at all. As QSGW gives the self-consistent solution at the scalar relativistic level, we add the spin-orbit operator, H_{SO}, as a perturbation (it is not included in the self-consistency cycle). The QSGW potential is mixed with LDA in the manner of Refs. 34 and 46. The resulting band structures for GaAs, AlAs, CdTe, and InSb are presented in Fig. 1. The band energies at high-symmetry points are presented in Table I and compared with experimental data and accurate empirical band calculations. The good agreement of calculated band energies with experimental values at all points of high symmetry indicates that the entire calculated band structure (ground- and excited-state quasiparticle energies and wave functions) is very close to that of the real materials throughout the entire BZ.

2. Supplementary data for the relativistic splitting

In Fig. 10 we show the evolution of the spin splitting as we look into larger parts of the BZ. We can see that whereas the maximum for the first conduction band is along the [110] direction for small regions around the Γ point, it is shifted toward the [210] direction as we move away from it.

In Fig. 11 we show the spin splitting together with three-dimensional plots of CB1 and CB2 bands of GaAs from two different viewing angles. It is clearly seen that the BZ regions with very high value of CB1 spin splitting are located close to the k points of CB1 and CB2 anticrossing.

[1] G. Dresselhaus, Phys. Rev. **100**, 580 (1955).
[2] R. C. Casella, Phys. Rev. **114**, 1514 (1959).
[3] L. C. Lew Yan Voon, M. Willatzen, M. Cardona, and N. E. Christensen, Phys. Rev. B **53**, 10703 (1996).
[4] Y. A. Bychkov and E. I. Rashba, Zh. Eksp. Teor. Fiz. Pis'ma Red. **39**, 66 (1984).
[5] L. C. Lew Yan Voon, M. Willatzen, P. V. Santos, M. Cardona, D. Munzar, and N. E. Christensen, Solid-State Electron. **40**, 191 (1996).
[6] A. T. Gorelenok, B. A. Marushchak, and A. N. Titkov, Izv. Akad. Nauk SSSR, Ser. Fiz. **50**, 290 (1986).
[7] D. Seiler, B. Bajaj, and A. Stevens, Phys. Rev. B **16**, 2822 (1977).
[8] R. Ranvaud, H. R. Trebin, U. Rössler, and F. H. Pollak, Phys. Rev. B **20**, 701 (1979).
[9] G. E. Pikus and G. L. Bir, Sov. Phys. Solid State **3**, 2221 (1962).
[10] W. Howlett and S. Zukotynski, Phys. Rev. B **16**, 3688 (1977).
[11] M. Cardona, N. E. Christensen, and G. Fasol, Phys. Rev. B **38**, 1806 (1988).
[12] O. Krupin, G. Bihlmayer, K. Starke, S. Gorovikov, J. E. Prieto, K. Döbrich, S. Blügel, and G. Kaindl, Phys. Rev. B **71**, 201403(R) (2005).
[13] S. F. Alvarado, H. Riechert, and N. E. Christensen, Phys. Rev. Lett. **55**, 2716 (1985).
[14] M. Cardona, N. E. Christensen, M. Dobrowolska, J. Furdyna, and S. Rodriguez, Solid State Commun. **60**, 17 (1986).
[15] C. Pidgeon and S. Groves, Phys. Rev. **186**, 824 (1969).
[16] W. Maier, G. Schmeider, and C. Klingshirn, Z. Phys. B: Condens. Matter **50**, 193 (1983).
[17] R. Sooryakumar, M. Cardona, and J. Merle, Solid State Commun. **48**, 581 (1983).
[18] T. Itoh, Y. Iwabuchi, and T. Kirihara, Phys. Status Solidi B **146**, 531 (1988).
[19] B. Jusserand, D. Richards, G. Allan, C. Priester, and B. Etienne, Phys. Rev. B **51**, 4707 (1995).
[20] M. Hruška, Š. Kos, S. A. Crooker, A. Saxena, and D. L. Smith, Phys. Rev. B **73**, 075306 (2006).
[21] L. Meier, G. Salis, I. Shorubalko, E. Gini, S. Schn, and K. Ensslin, Nat. Phys. **3**, 650 (2007).
[22] R. Winkler, *Spin-Orbit Coupling Effects in Two-Dimensional Electron and Hole Systems*, Springer Tracts in Modern Physics Vol. 191 (Springer-Verlag, Berlin, 2003).
[23] S. LaShell, B. A. McDougall, and E. Jensen, Phys. Rev. Lett. **77**, 3419 (1996).
[24] E. Rotenberg and S. D. Kevan, Phys. Rev. Lett. **80**, 2905 (1998).
[25] M. I. Dyakonov and V. I. Perel, Sov. Phys. JETP **33**, 1053 (1971).
[26] D. V. Bulaev and D. Loss, Phys. Rev. B **71**, 205324 (2005).
[27] A. N. Chantis, K. D. Belashchenko, E. Y. Tsymbal, and M. van Schilfgaarde, Phys. Rev. Lett. **98**, 046601 (2007).
[28] J. Moser, A. Matos-Abiague, D. Schuh, W. Wegscheider, J. Fabian, and D. Weiss, Phys. Rev. Lett. **99**, 056601 (2007).
[29] P. D. Dresselhaus, C. M. A. Papavassiliou, R. G. Wheeler, and R. N. Sacks, Phys. Rev. Lett. **68**, 106 (1992).
[30] B. A. Bernevig and S.-C. Zhang, Phys. Rev. Lett. **96**, 106802 (2006).
[31] E. Bauer, G. Hilscher, H. Michor, C. Paul, E. W. Scheidt, A. Gribanov, Y. Seropegin, H. Noël, M. Sigrist, and P. Rogl, Phys. Rev. Lett. **92**, 027003 (2004).
[32] S. Fujimoto, J. Phys. Soc. Jpn. **76**, 051008 (2007).
[33] M. P. Surh, M. F. Li, and S. G. Louie, Phys. Rev. B **43**, 4286 (1991).
[34] A. N. Chantis, M. van Schilfgaarde, and T. Kotani, Phys. Rev. Lett. **96**, 086405 (2006).
[35] J. W. Luo, G. Bester, and A. Zunger, Phys. Rev. Lett. **102**, 056405 (2009).
[36] M. van Schilfgaarde, T. Kotani, and S. Faleev, Phys. Rev. Lett. **96**, 226402 (2006).
[37] T. Kotani, M. van Schilfgaarde, and S. V. Faleev, Phys. Rev. B **76**, 165106 (2007).
[38] O. K. Andersen, Phys. Rev. B **12**, 3060 (1975).
[39] M. Methfessel, M. van Schilfgaarde, and R. A. Casali, *Lecture Notes in Physics* (Springer-Verlag, Berlin, 2000), Vol. 535.
[40] A. N. Chantis, M. van Schilfgaarde, and T. Kotani, Phys. Rev. B **76**, 165126 (2007).
[41] T. Kotani, M. van Schilfgaarde, S. V. Faleev, and A. N. Chantis, J. Phys.: Condens. Matter **19**, 365236 (2007).
[42] A. N. Chantis, R. C. Albers, M. D. Jones, M. van Schilfgaarde, and T. Kotani, Phys. Rev. B **78**, 081101(R) (2008).
[43] A. N. Chantis, R. C. Albers, N. E. Christensen, and A. Svane, Philos. Mag. **89**, 1801 (2009).
[44] K. V. Samokhin, E. S. Zijlstra, and S. K. Bose, Phys. Rev. B **69**, 094514 (2004).
[45] M. van Schilfgaarde, T. Kotani, and S. V. Faleev, Phys. Rev. B **74**, 245125 (2006).
[46] A. N. Chantis, M. Cardona, N. E. Christensen, D. L. Smith, M. van Schilfgaarde, T. Kotani, A. Svane, and R. C. Albers, Phys. Rev. B **78**, 075208 (2008).
[47] A.-B. Chen and A. Sher, *Semiconductors Alloys, Physics and Materials Engineering* (Plenum Press, New York, 1995).
[48] M. Cardona and M. L. W. Thewalt, Rev. Mod. Phys. **77**, 1173 (2005).
[49] P. Carrier and S.-H. Wei, Phys. Rev. B **70**, 035212 (2004).